ACADEMIC PRESS

Available online at www.sciencedirect.com

SCIENCE DIRECT®

Journal of Sound and Vibration 269 (2004) 823–852

JOURNAL OF SOUND AND VIBRATION

www.elsevier.com/locate/jsvi

Three-dimensional non-linear coupling and dynamic tension in the large-amplitude free vibrations of arbitrarily sagged cables

Narakorn Srinil[a], Giuseppe Rega[b], Somchai Chucheepsakul[a,*]

[a] *Department of Civil Engineering, King Mongkut's University of Technology Thonburi, 48 Bangmod, Toongkru, Bangkok 10140, Thailand*

[b] *Dipartimento di Ingegneria Strutturale e Geotecnica, Universita' di Roma La Sapienza, via A. Gramsci, 53 Roma 00197, Italy*

Received 24 May 2002; accepted 23 January 2003

Abstract

This paper presents a model formulation capable of analyzing large-amplitude free vibrations of a suspended cable in three dimensions. The virtual work-energy functional is used to obtain the non-linear equations of three-dimensional motion. The formulation is not restricted to cables having small sag-to-span ratios, and is conveniently applied for the case of a specified end tension. The axial extensibility effect is also included in order to obtain accurate results. Based on a multi-degree-of-freedom model, numerical procedures are implemented to solve both spatial and temporal problems. Various numerical examples of arbitrarily sagged cables with large-amplitude initial conditions are carried out to highlight some outstanding features of cable non-linear dynamics by accounting also for internal resonance phenomena. Non-linear coupling between three- and two-dimensional motions, and non-linear cable tension responses are analyzed. For specific cables, modal transition phenomena taking place during in-plane vibrations and ensuing from occurrence of a dominant internal resonance are observed. When only a single mode is initiated, a higher or lower mode can be accommodated into the responses, making cable spatial shapes hybrid in some time intervals.

1. Introduction

Cable systems are of great interest in a wide range of practical applications for supplying both support and stability to large structures. Moreover, they are of interest from a theoretical point of

*Corresponding author. Tel.: +662-470-9134-36; fax: +662-427-9063.

E-mail addresses: narakorns@hotmail.com (N. Srinil), giuseppe.rega@uniroma1.it (G. Rega), somchai.chu@kmutt.ac.th (S. Chucheepsakul).

0022-460X/03/$ - see front matter
doi:10.1016/S0022-460X(03)00137-8

view, owing to many fundamental non-linear phenomena induced by the overall slenderness and inherent flexibility of cable structural systems. As a result of dynamical susceptibility to excitation from surrounding mediums, cable vibrations of large amplitudes may happen in some circumstances, and may eventually degrade the system performance. To reach a fundamental understanding of cable behaviors, three-dimensional (3-D) modelling and geometrically non-linear characteristics should be fully accounted for in the analysis.

Non-linear free vibrations of a suspended cable have been investigated by a number of researchers, which include Hagedorn and Schafer [1], Luongo et al. [2,3], Rega et al. [4], and Benedettini et al. [5]. All of them deal with simple cable models, with one or two degrees of freedom, developed and utilized to obtain analytical solutions. In the same theoretical framework, both single-degree-of-freedom [6,7] and multi-degree-of-freedom (m.d.o.f.) [8–12] models have been considered to explore numerous non-linear phenomena arising in cable forced vibrations. These include the meaningful effects of non-linear modal coupling under various external/internal resonance conditions and the possibility of non-periodic responses. The richness of cable non-linear dynamics has been further highlighted through systematic experimental investigations [13,14]. In all theoretical models, a certain number of assumptions have been introduced to simplify the analytical treatment. Namely, the initial static strain is disregarded so as to obtain an inextensible parabolic profile of the cable equilibrium configuration where the sag-to-span ratio is of the order of $\frac{1}{8}$ or less. Moreover, the dynamic tension is defined as a function of time only, thus being spatially uniform, which ensues from the inertial force in the longitudinal direction being neglected according to a quasi-static stretching model of the cable in motion.

However, Behbahani-Nejad and Perkins [15] have illustrated that the analysis of tension waves propagating freely along the cable length cannot be accomplished using simple models. Pakdemirli et al. [16] and Rega et al. [17] have documented that the results obtained by analyzing reduced-mode discretized models of cable may be quantitatively erroneous for cables with non-zero sag. Moreover, several studies have highlighted how, depending on system elasto-geometric properties, the effect of axial deformation on the dynamic behaviors can be significant and should be considered in the analysis [18–24]. For arbitrarily supported cables or cables with large curvature, the investigation may require further numerical implementations [25,26]. Takahashi and Konishi [27] examined sagged cables with either horizontal or inclined supports qualitatively, and discussed geometrically non-linear effects, but they overlooked the significance of cable extensibility. Recently, Luo and Mote [28] developed a comprehensive 3-D model governing the steady response of a travelling, arbitrarily sagged, elastic cable, and obtained exact, closed-form solutions for steady motion under various loadings. Nevertheless, it seems worth investigating further 3-D non-linear coupling, as well as the variability of dynamic tension during vibration, by considering a m.d.o.f. model which accounts for cable extensibility and non-uniform dynamic tension, and which is not restricted to low values of the sag-to-span ratios.

The objective of the present study is to analyze numerically the large-amplitude free vibrations of arbitrarily sagged elastic cables through a rigorous formulation, which takes into account the axial deformation effect. Based on the principle of virtual work-energy, the non-linear equations of 3-D coupled motions are derived in Section 2. A m.d.o.f. model, which is not limited to cables having small sag-to-span ratios, is utilized within a numerical solution of the spatial and temporal problems (Section 3). The attention is then placed on the investigation of the cable 3-D non-linear free dynamics ensuing from a given set of initial conditions (Section 4). With this aim, the linear

modal coordinates of each vibration mode achieved from the previous study of Chucheepsakul and Srinil [24] are assumed as initial conditions for spatial displacements. The aim is to analyze: (i) how the cable non-linear response evolves, also in terms of dynamic tension; (ii) how significant the coupling of 3-D motion is; and (iii) whether and how the internal resonance conditions affect the dynamics. The non-linear free vibration characteristics of out-of-plane and in-plane vibrations are examined comprehensively and are discussed in detail.

2. Derivation of equations of motion

Fig. 1 displays the typical reference configuration of a suspended cable of horizontal span X_H with two immovable pinned-supports at the same ground level. One end of the cable is fixed while the other one is the position where the specified tension T_H is applied to maintain the cable in its static configuration. The coordinates of any point along the cable are represented using the Cartesian system. Three different states of cable configuration are distinguished, namely the unstretched, the equilibrium and the dynamic states. The cable forms a catenary suspension under its own weight at the initial unstretched state (x, y). Due to axial stretching, the cable moves to the equilibrium position (x_0, y_0), which is considered as the initial configuration for cable dynamics. Owing to disturbances from external excitation, the cable then moves to the dynamic or displaced state, in which u, v and w are the components of displacement measured from the equilibrium configuration in the direction of X-, Y- and Z-axis, respectively.

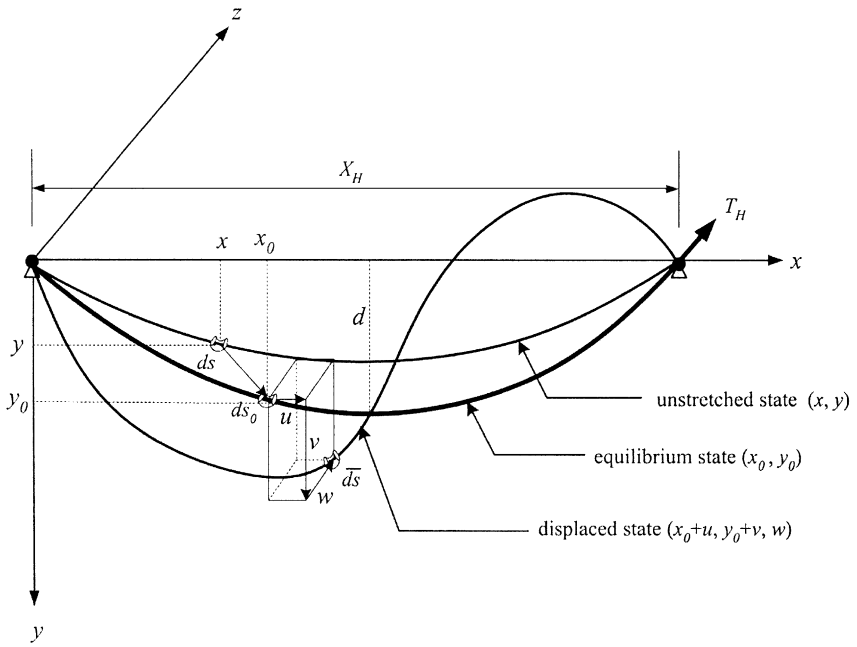

Fig. 1. Reference configurations of a suspended cable.

The length $\mathrm{d}s_0$ of an infinitesimal cable element at the equilibrium state can be written as

$$\mathrm{d}s_0 = \sqrt{1 + y_0'^2}\,\mathrm{d}x_0, \tag{1}$$

where a superscript prime denotes a differentiation with respect to x_0. Using Lagrangian-strain definition, the cable segments at the unstretched state $\mathrm{d}s$ and displaced state $\mathrm{d}\bar{s}$ are expressed, respectively, as

$$\mathrm{d}s = \frac{\sqrt{1 + y_0'^2}}{1 + \varepsilon_0}\,\mathrm{d}x_0, \tag{2}$$

$$\mathrm{d}\bar{s} = \sqrt{(1 + u')^2 + (y_0' + v')^2 + w'^2}\,\mathrm{d}x_0, \tag{3}$$

in which ε_0 is the initial static strain. The total strain at the displaced state is

$$\bar{\varepsilon} = \frac{(1 + \varepsilon_0)}{\sqrt{1 + y_0'^2}}\sqrt{(1 + u')^2 + (y_0' + v')^2 + w'^2} - 1. \tag{4}$$

The strain energies caused by bending, torsional and shear rigidities are neglected based on the assumption of a perfectly flexible cable. Hence, the strain energy is due only to the stretching of the cable axis. In view of the application of the principle of virtual work, the strain energy variation is written as

$$\delta U = \int_0^S EA\bar{\varepsilon}\delta\bar{\varepsilon}\,\mathrm{d}s, \tag{5}$$

where S is the total undeformed arc-length, E Young's modulus of the cable, and A its cross-sectional area, which is assumed to be constant. Substituting Eq. (4) and its variational expression into Eq. (5) yields

$$\delta U = \int_0^{X_H} \left\{ \begin{array}{l} \left(\dfrac{EA(1 + \varepsilon_0)(1 + u')}{\sqrt{1 + y_0'^2}} - \dfrac{EA(1 + u')}{\sqrt{(1 + u')^2 + (y_0' + v')^2 + w'^2}} \right) \delta u' + \\ \left(\dfrac{EA(1 + \varepsilon_0)(y_0' + v')}{\sqrt{1 + y_0'^2}} - \dfrac{EA(y_0' + v')}{\sqrt{(1 + u')^2 + (y_0' + v')^2 + w'^2}} \right) \delta v' + \\ \left(\dfrac{EA(1 + \varepsilon_0)(w')}{\sqrt{1 + y_0'^2}} - \dfrac{EA\,w'}{\sqrt{(1 + u')^2 + (y_0' + v')^2 + w'^2}} \right) \delta w' \end{array} \right\} \mathrm{d}x_0. \tag{6}$$

The virtual work done by the cable weight w_C per unit unstretched length is expressed as

$$\delta W_e = \int_0^{X_H} \frac{w_C\sqrt{1 + y_0'^2}}{1 + \varepsilon_0}\,\mathrm{d}x_0\,\delta v. \tag{7}$$

In turn, the virtual work done by the inertial forces is given by

$$\delta W_i = -\int_0^{X_H} \frac{w_C\sqrt{1+y_0'^2}}{g(1+\varepsilon_0)}(\ddot{u}\delta u + \ddot{v}\delta v + \ddot{w}\delta w)\,\mathrm{d}x_0, \tag{8}$$

where $w_C\sqrt{1+y_0'^2}/g(1+\varepsilon_0)$ is the cable mass per unit stretched length, g is the gravitational force, $\ddot{u}, \ddot{v}$ and $\ddot{w}$ are the accelerations in the direction of X-, Y- and Z-axis, respectively. Utilizing the standard principle of virtual displacement, the total virtual work-energy of the cable system is expressed as

$$\delta\Pi = \delta U - (\delta W_e + \delta W_i) = 0. \tag{9}$$

After substitution of Eqs. (6)–(8) into Eq. (9), and integration by parts of the latter with application of the boundary conditions $\delta u = \delta v = \delta w = 0$ at $x_0 = 0$ and $x_0 = X_H$, Euler's equations associated with the virtual displacements $\delta u, \delta v$ and δw read, respectively:

$$\left(\frac{EA(1+\varepsilon_0)(1+u')}{\sqrt{1+y_0'^2}} - \frac{EA(1+u')}{\sqrt{(1+u')^2+(y_0'+v')^2+w'^2}}\right)' - \frac{w_C\sqrt{1+y_0'^2}}{g(1+\varepsilon_0)}\ddot{u} = 0, \tag{10}$$

$$\left(\frac{EA(1+\varepsilon_0)(y_0'+v')}{\sqrt{1+y_0'^2}} - \frac{EA(y_0'+v')}{\sqrt{(1+u')^2+(y_0'+v')^2+w'^2}}\right)' - \frac{w_C\sqrt{1+y_0'^2}}{g(1+\varepsilon_0)}\ddot{v} + \frac{w_C\sqrt{1+y_0'^2}}{1+\varepsilon_0} = 0, \tag{11}$$

$$\left(\frac{EA(1+\varepsilon_0)(w')}{\sqrt{1+y_0'^2}} - \frac{EA\,w'}{\sqrt{(1+u')^2+(y_0'+v')^2+w'^2}}\right)' - \frac{w_C\sqrt{1+y_0'^2}}{g(1+\varepsilon_0)}\ddot{w} = 0. \tag{12}$$

By substituting the equilibrium conditions $u = v = w = u' = v' = w' = u'' = v'' = w'' = \ddot{u} = \ddot{v} = \ddot{w} = 0$ into Eqs. (10)–(12), one can obtain Euler's equations corresponding to the equilibrium state in the direction of virtual displacements δu and δv:

$$\left(EA\,\varepsilon_0/\sqrt{1+y_0'^2}\right)' = 0, \tag{13}$$

$$\left(EA\,\varepsilon_0 y_0'/\sqrt{1+y_0'^2}\right)' + w_C\sqrt{1+y_0'^2}/(1+\varepsilon_0) = 0. \tag{14}$$

Subtracting Eq. (10) by Eq. (13), and Eq. (11) by Eq. (14), the governing equations of motion corresponding to the displacements in the directions u, v and w, respectively, are

$$\left(\frac{EA + EA(1+\varepsilon_0)u'}{\sqrt{1+y_0'^2}} - \frac{EA(1+u')}{\sqrt{(1+u')^2+(y_0'+v')^2+w'^2}}\right)' = \frac{w_C\sqrt{1+y_0'^2}}{g(1+\varepsilon_0)}\ddot{u}, \tag{15}$$

$$\left(\frac{EAy_0' + EA(1+\varepsilon_0)v'}{\sqrt{1+y_0'^2}} - \frac{EA(y_0'+v')}{\sqrt{(1+u')^2+(y_0'+v')^2+w'^2}}\right)' = \frac{w_C\sqrt{1+y_0'^2}}{g(1+\varepsilon_0)}\ddot{v}, \tag{16}$$

$$\left(\frac{EA(1+\varepsilon_0)w'}{\sqrt{1+y_0'^2}} - \frac{EA(w')}{\sqrt{(1+u')^2+(y_0'+v')^2+w'^2}}\right)' = \frac{w_C\sqrt{1+y_0'^2}}{g(1+\varepsilon_0)}\ddot{w}. \tag{17}$$

These equations are highly non-linear and are coupled through the cable equilibrium configuration. The associated boundary conditions read

$$u(0,t) = v(0,t) = w(0,t) = u(X_H,t) = v(X_H,t) = w(X_H,t) = 0. \tag{18}$$

This system is useful for analyzing 3-D undamped large-amplitude free vibrations under specified initial conditions. It is worth noticing that the formulation considered could be accounted for also in a local coordinate reference frame by using the relevant coordinate transformation relationship [24] or suitable Euler-angle formulations [22].

3. Method of solution

Cable equilibrium configuration is to be evaluated. The shooting method is used to solve the non-linear equilibrium Eqs. (13) and (14). Since a specified tension is imposed at one end of the cable, in the computation it is more convenient to use an expression for the tension at any point along the cable in place of Eq. (14). For this purpose, the equilibrium condition of a cable segment in the tangential direction is used and is then converted into the following integral expression:

$$T(x_0) = T_H - \int_{X_H}^{X_0} \frac{w_C}{(1+\varepsilon_0)} y_0' \, \mathrm{d}x_0. \tag{19}$$

Using Eqs. (13) and (19), the proposed algorithm reveals itself to be efficient for solving the cable problem with a specified end tension [29]. Each step of spatial integration is performed through the fourth order Runge–Kutta scheme.

In order to analyze the free vibration problem, each partial differential equation (Eqs. (15)–(17)) is differentiated term by term with respect to the spatially independent variable x_0. The ensuing equations of motion are written as follows:

$$(\Theta/\Psi)u'' + (1/\Psi)F(u', u'', v', v'', w', w'') = \ddot{u}, \tag{20}$$

$$(\Theta/\Psi)v'' + (1/\Psi)G(u', u'', v', v'', w', w'') = \ddot{v}, \tag{21}$$

$$(\Theta/\Psi)w'' + (1/\Psi)H(u', u'', v', v'', w', w'') = \ddot{w}, \tag{22}$$

where the spatial variables $\Theta = (1+\varepsilon_0)/\sqrt{(1+y_0'^2)}$ and $\Psi = w_C\sqrt{1+y_0'^2}/EA\,g(1+\varepsilon_0)$ are defined, and the functions $F(..)$, $G(..)$ and $H(..)$ of the displacement variables read:

$$F(..) = \left\{ \begin{array}{c} \left[\dfrac{\varepsilon_0' u'}{(1+y_0'^2)^{1/2}} - \dfrac{(1+u'+\varepsilon_0 u')y_0' y_0''}{(1+y_0'^2)^{3/2}}\right] \\ -\left[\dfrac{(y_0'+v')^2 u'' + w'^2 u'' - (1+u')(y_0'+v')(y_0''+v'') - (1+u')w'w''}{((1+u')^2+(y_0'+v')^2+w'^2)^{3/2}}\right] \end{array} \right\}, \tag{23}$$

$$G(..) = \left\{ \begin{array}{c} \left[\dfrac{y_0'' + \varepsilon_0' v'}{(1+y_0'^2)^{1/2}} - \dfrac{(y_0'+v'+\varepsilon_0 v')y_0' y_0''}{(1+y_0'^2)^{3/2}}\right] \\ -\left[\dfrac{(1+u')^2(y_0''+v'') + w'^2(y_0''+v'') - (1+u')(y_0'+v')u'' - (y_0'+v')w'w''}{\left((1+u')^2+(y_0'+v')^2+w'^2\right)^{3/2}}\right] \end{array} \right\}, \tag{24}$$

$$H(..) = \left\{ \begin{array}{c} \left[\dfrac{\varepsilon_0' w'}{(1+y_0'^2)^{1/2}} - \dfrac{(w'+\varepsilon_0 w')y_0' y_0''}{(1+y_0'^2)^{3/2}}\right] \\ -\left[\dfrac{(1+u')^2 w'' + (y_0'+v')^2 w'' - w'(1+u')u'' - w'(y_0'+v')(y_0''+v'')}{((1+u')^2+(y_0'+v')^2+w'^2)^{3/2}}\right] \end{array} \right\}. \tag{25}$$

Numerical solutions to Eqs. (20)–(22) were obtained using finite difference discretization in both space and time. Central differences were used for approximating spatial derivatives and the second temporal derivatives. This led to a simple explicit form of the equations of motion for a solution of the unknown displacements. The obtained displacements were then utilized as initial guess of the next process by means of a predictor–corrector iterative algorithm. The solution over each time step was iterated repeatedly until the convergence was satisfactory, and the allowable tolerance was accomplished by the criterion of the second order vector norm.

4. Numerical results and discussions

A long suspended cable with horizontal span $X_H = 850\,\mathrm{m}$ is analyzed in order to better highlight the effect of strain variation on non-linear dynamics. The cable has a cross-sectional area $A = 0.1159\,\mathrm{m}^2$, cable density equal to $8337.9\,\mathrm{kg/m}^3$, and modulus of elasticity $E = 1.794\times10^7\,\mathrm{kN/m}^2$. The cable is discretized into 50 segments. Integration was performed in all cases with a time step equal to 0.00001. The linear eigenvector is evaluated and normalized in such a way that the maximum amplitude of nodal displacement is equal to unity [24]. Subsequently, each nodal displacement is multiplied by the initial amplitude (Δ) specified in each case. Without structural damping, this amplitude has been chosen to attain a moderately large value to ensure that the summation of the cable static tension and the additional dynamic one does not become a compressive force. The initial velocities for all directions are assumed to be identically zero throughout the present study.

Table 1
Cable properties and corresponding linear frequencies for four different cables

Cable	λ/π	T_H (kN)	ε_m	d (m)	S (m)	S_0 (m)	Linear natural frequencies (Hz)					
							Out-of-plane mode: O		In-plane mode: I			
							1st S–O	1st A–O	1st S–I	1st A–I	2nd S–I	2nd A–I
A	0.72	30 000	0.01443	28.39	840.48	852.53	0.104	0.208	0.123	0.206	0.312	0.414
B	2.00	15 642	0.00752	56.59	853.69	859.96	0.074	0.147	0.145	0.145	0.226	0.292
C	4.00	10 500	0.00505	89.57	870.51	874.67	0.058	0.115	0.158	0.112	0.222	0.229
D	10.01	7000	0.00337	164.11	926.65	929.31	0.043	0.085	0.119	0.076	0.206	0.165

S: symmetric mode; A: antisymmetric mode.

Table 1 gives the physical properties of four different cables, including the specified end tension T_H, maximum static strain ε_m, cable sag d, cable unstretched length S and cable equilibrium length S_0, which are all governed by the unique cable parameter governing the linear frequency spectrum [20,30], i.e., $\lambda/\pi = \sqrt{(w_C S_0)^2 EA/T_a^3}/\pi$ (T_a is the static tension at cable mid-span). The corresponding linear out-of-plane and in-plane frequencies are also documented. The specified tensions have been selected to guarantee the existence of 1:1 internal resonance conditions between symmetric and antisymmetric in-plane frequencies at the first and second crossover points in the spectrum ($\lambda/\pi = 2$, 4 for cables B and C, respectively), in comparison with non-crossover points (cables A and D). By altering this specified tension, the influence of cable extensibility (strain variation) and cable sag can be seen. Obviously, the maximum extensibility is that of cable A, whereas the maximum sag is that of cable D. Emphasis is placed on a prescribed initial displacement condition according to the first four natural modes, namely the first symmetric and antisymmetric modes of the in-plane and out-of-plane vibrations. Attention is focused, on one side, on crossover cables, whose actual dynamic behaviors are analyzed versus the background of theoretical conditions for activation of the existing internal resonances obtained within an infinite dimensional analytical framework [31]; on the other side, attention is focused on a large sag cable exhibiting higher multi-mode and axial extensibility effects. The analysis is performed basically in terms of time histories of dynamic responses. In addition, spatial or phase-portrait representations of cable motion and frequency response measures are provided to describe specific features of system dynamics.

The 3-D non-linear responses at mid and quarter spans non-dimensionalized by the horizontal span (X_H) are typically shown. Time (T) is non-dimensionalized by the fundamental period of each linear frequency. The cable total tension $T_D = EA\,\bar{\varepsilon}$ is readily computed from the displacements through Eq. (4), and is then non-dimensionalized by the value of the maximum static tension (T_H). Total tension responses inclusive of the initial static strain are presented rather than simple additional dynamic tension. Moreover, not only the maximum tension—which is of interest to the designer for evaluating the tensile strength capability—is investigated, but also the minimum tension so as to search for the position where compression possibly happens. The dynamic strain being a function of both space and time, the positions at which maximum and minimum tensions occur may change, depending on how the nodal points vibrate in each time step.

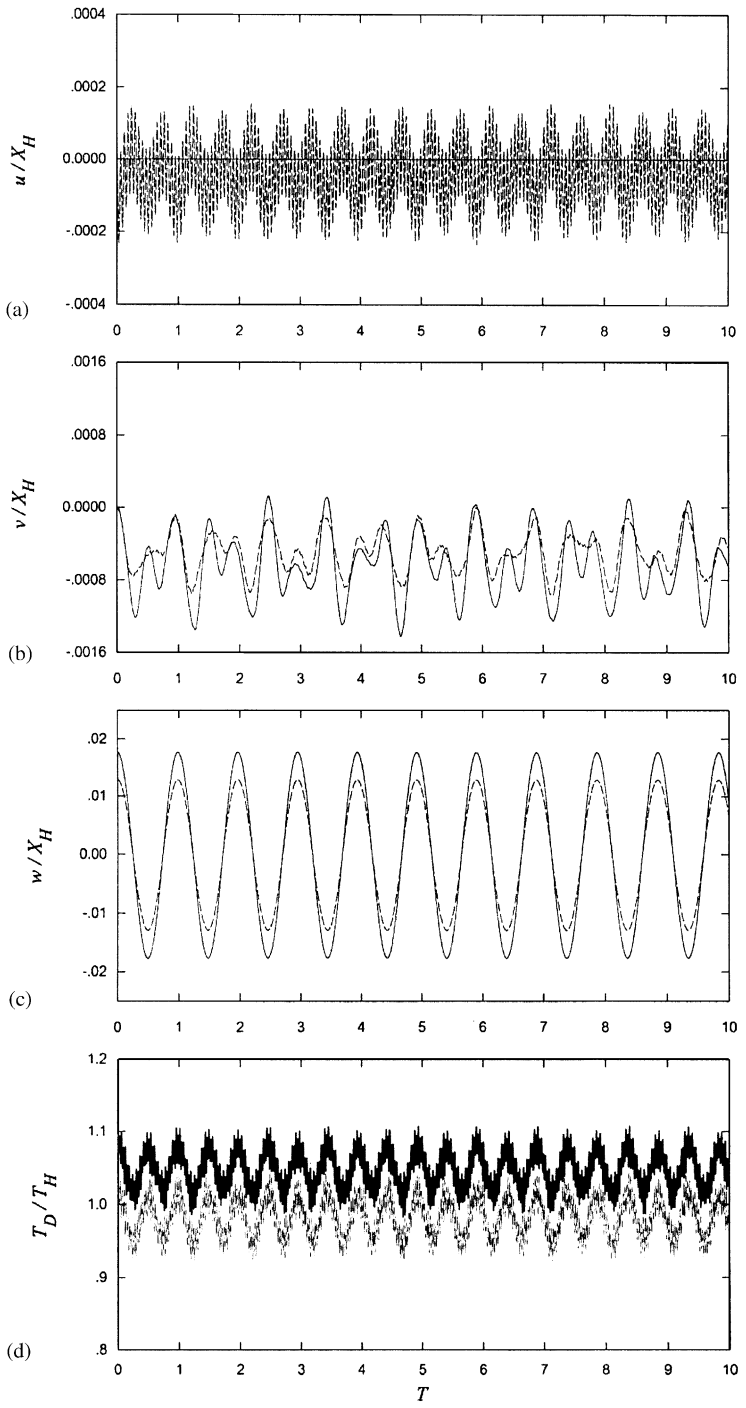

Fig. 2. Dynamic responses of cable A under initial condition of the 1st S–O mode: (a) longitudinal response; (b) vertical response; (c) out-of-plane response: —— mid-span, – – – quarter span; (d) cable tension response: —— maximum, – – – minimum

4.1. Large-amplitude out-of-plane free vibrations

The analysis starts by considering out-of-plane initial conditions with either symmetric or antisymmetric spatial shapes.

4.1.1. First symmetric out-of-plane mode (1st S–O mode)

The assigned amplitude Δ is equal to 15 m for each cable. Starting from taut cable A, the out-of-plane response is perfectly periodic (Fig. 2(c)). The energy driven by the out-of-plane response geometrically induces longitudinal and vertical responses through kinematic coupling of 3-D motion. The vertical non-periodic response is disturbed by a higher frequency (Fig. 2(b)), while the longitudinal one has a considerably lower amplitude (Fig. 2(a)). The out-of-plane motion does not involve any first order cable stretching in the linear theory [30], corresponding substantially to a pendulum-like motion. In contrast, Fig. 2(d) displays the additional forces induced in the non-linear range.

Cable B corresponds to the first crossover ($\lambda/\pi = 2$), where various internal resonances do coexist. However, the meaningful one involving the initiated out-of-plane mode is the 2:1 resonance between 1st S–I and 1st S–O modes, which is actually activable due to non-orthogonality of the relevant non-linear normal modes, which are both symmetric [31]. Consistently, a beating phenomenon is observed in the relevant responses (Fig. 3), as already highlighted in Ref. [5] for a two-degree-of-freedom cable model. The maximum out-of-plane amplitude decreases to about 0.64 times its initial value (Fig. 3(c)) due to the interaction with the corresponding in-plane response, whose maximum amplitude rises from zero to about 43.74% of the maximum out-of-plane amplitude. Correspondingly, the cable maximum tensions in Fig. 3(d) are enhanced considerably, and are greater than those obtained for cable A, being associated mostly with the increased in-plane vibration (Fig. 2(d)). The relationship between vertical and out-of-plane displacements at mid-span is depicted in Fig. 4(a). It can be seen that the out-of-plane component vibrates nearly symmetrically about the in-plane axis. The in-plane amplitude reaches the maximum negative value when the out-of-plane amplitude is close to zero. This implies that the cable configuration drifts upwards when the cable vibrates close to the vertical plane, as shown by the cable 3-D profiles in Fig. 4(b) for $T \approx 0 - 5$.

Consider now cable D sagging significantly ($d/X_H \approx 1/5$). The relevant longitudinal and vertical responses contain many high-frequency components and are definitely non-periodic (Figs. 5(a) and (b)), whereas the out-of-plane response in Fig. 5(c) is still periodic. The maximum amplitude of tension response is lower than that obtained for the resonant cable B. Since the out-of-plane response of each cable has a single (low) frequency, the Fourier amplitude spectral densities of the driven vertical responses are illustrated in Fig. 6 against those of cables A and B, in order to check the dominant frequency of the vibrations. Evidently, the vertical responses of cables A and D contain a number of higher frequency components (Figs. 6(a) and (c)) relevant to their non-periodic nature. In contrast, cable B attains a single frequency (0.156 Hz) twice that of the out-of-plane one (0.078 Hz), due to the energy being periodically transferred between the driving and excited modes of the 2:1 resonant cable (Fig. 6(b)).

It is worth analyzing the spatial shape of non-periodic responses by focusing attention on the large sag cable D, whose longitudinal, vertical and transversal vibration profiles at different instants ($T \approx 6.0 - 6.5$) are illustrated in Fig. 7. Apparently, the in-plane response profiles manifest

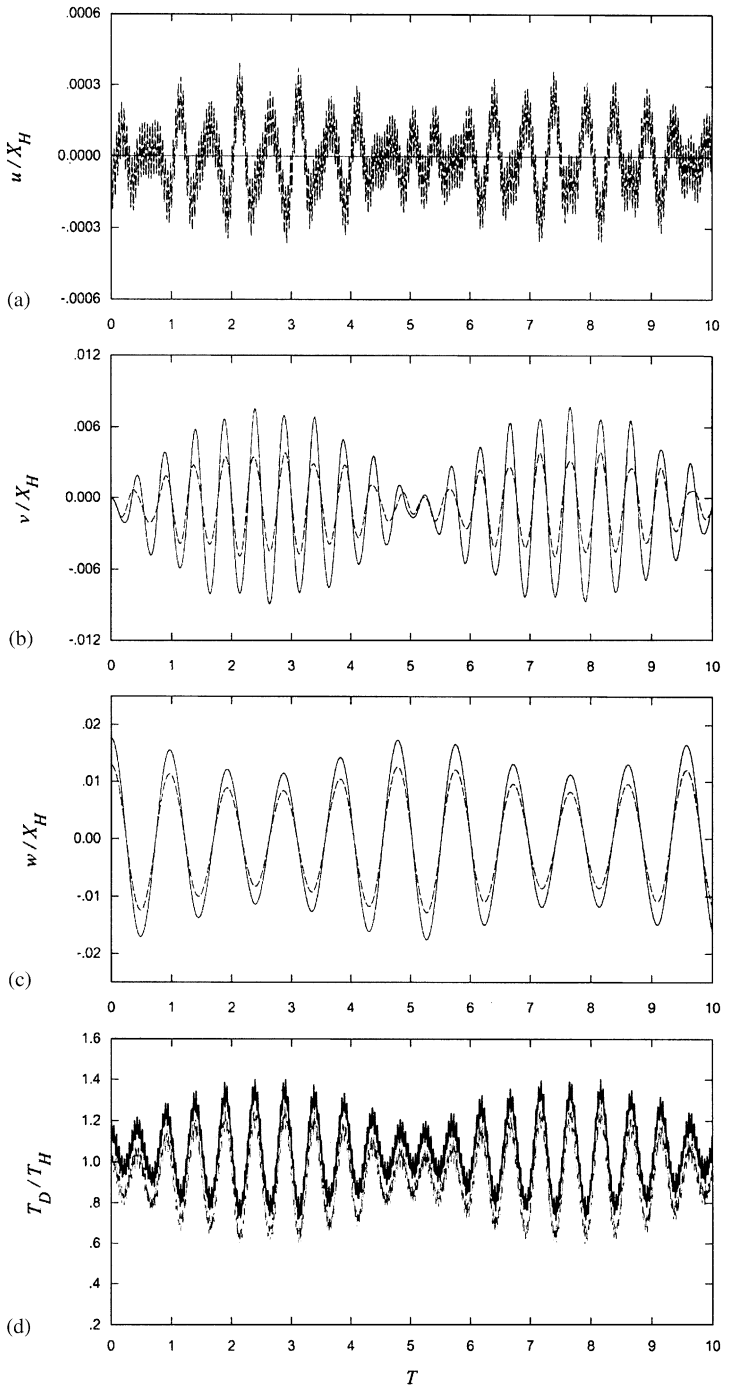

Fig. 3. Dynamic responses of cable B under initial condition of the 1st S–O mode: (a) longitudinal response; (b) vertical response; (c) out-of-plane response: —— mid-span, – – – quarter span; (d) cable tension response: —— maximum, – – – minimum.

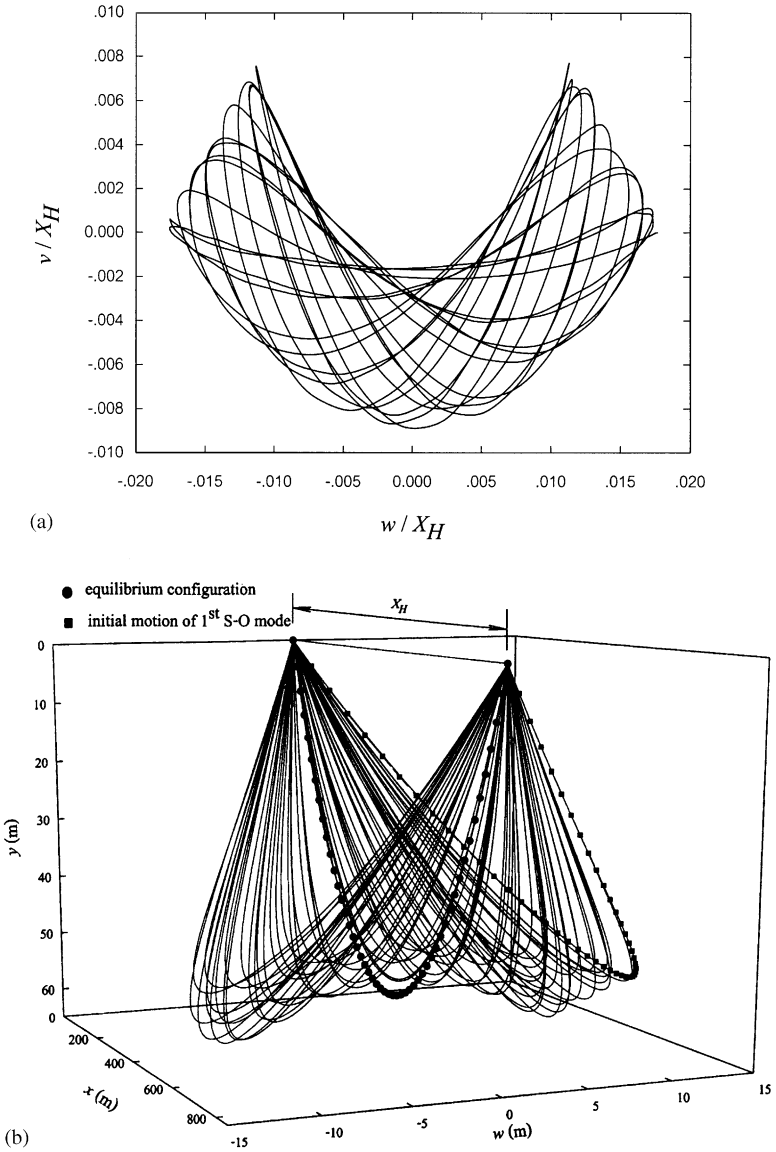

Fig. 4. Response of cable B under initial condition of the 1st S–O mode: (a) relationship plot between vertical and out-of-plane displacements at mid-span; (b) 3-D profiles ($T \approx 0-5$).

themselves as a combination of contributions from many modes (Figs. 7(a) and (b)), different from the nearly unimodal out-of-plane profile (Fig. 7(c)). Because of the high modal densities of cable suspensions, significant higher order in-plane modes are generated when a single-mode out-of-plane amplitude is initiated. This multi-harmonic character of the driven in-plane response occurs even for the shallower cables, though to a minor extent. This highlights the need of utilizing a m.d.o.f. cable model in order to obtain detailed and reliable non-linear response predictions, mostly for a relatively large sag cable.

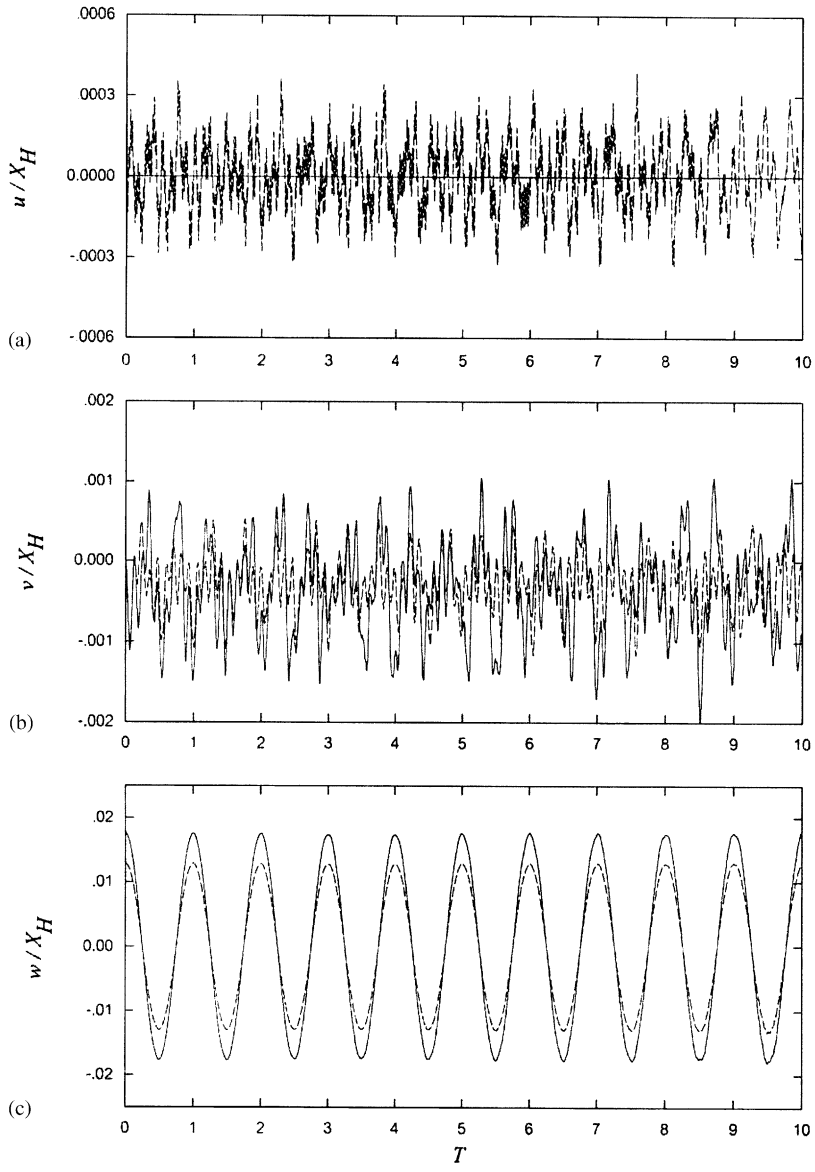

Fig. 5. Dynamic responses of cable D under initial condition of the 1st S–O mode: (a) longitudinal response; (b) vertical response; (c) out-of-plane response: —— mid-span, – – – quarter span.

4.1.2. *First antisymmetric out-of-plane mode (1st A–O mode)*

For cable B with $\Delta = 15\,\mathrm{m}$, the longitudinal and vertical displacements—the former still exhibiting much lower amplitude values—are disturbed by high-frequency components. The in-plane response is that of the 2nd S–I mode, which is supposed to be excited according to a super-harmonic coupling (of the order of $\frac{3}{2}$ approximately) induced by the driving 1st A–O mode, whereas the out-of-plane response is perfectly periodic and its maximum amplitude is of course greater than that occurring at quarter-span when exciting the 1st S–O mode (Fig. 3(c)).

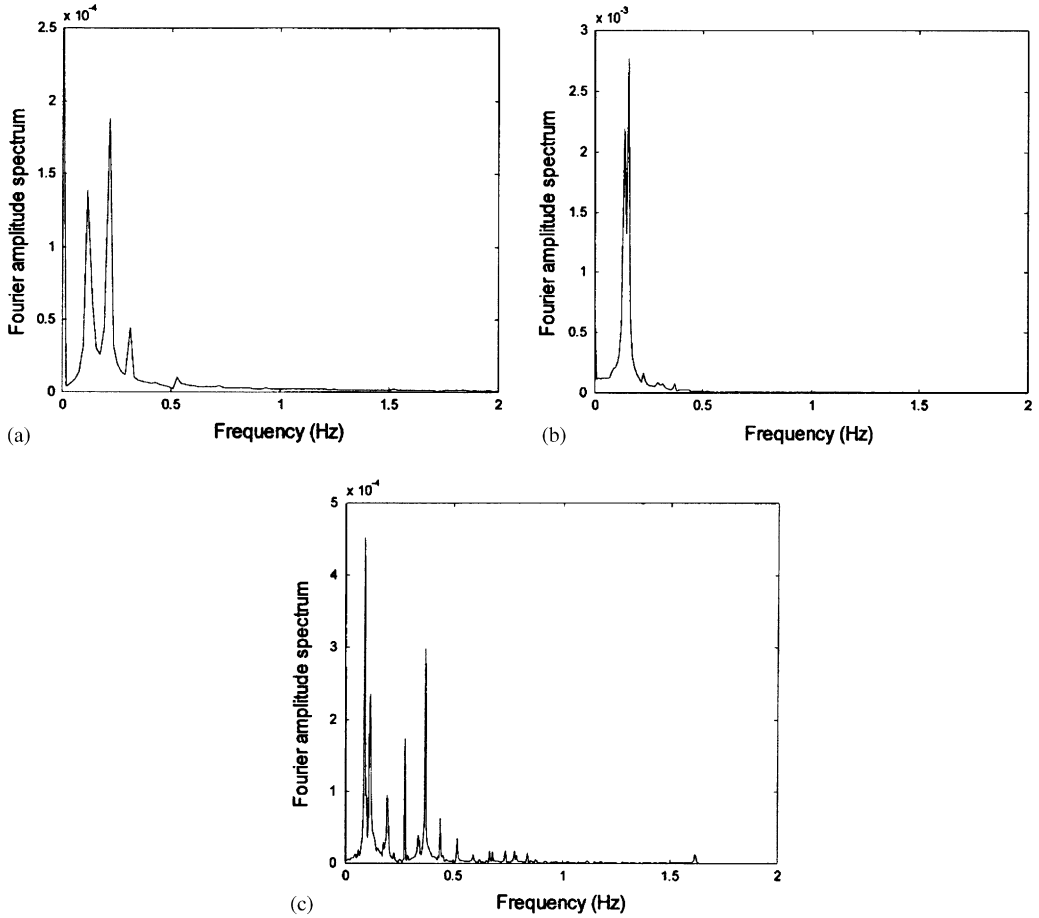

Fig. 6. Fourier amplitude spectra of cable vertical responses under initial condition of the 1st S–O mode: (a) cable A; (b) cable B; (c) cable D.

When considering cable C with $\Delta = 5\,\mathrm{m}$, the beating phenomenon is observed again for the overall responses (Fig. 8), resembling that obtained for the first resonant cable B in Fig. 3. The associated cable parameter is that of the second crossover where various frequency commensurabilities do occur. Amongst them, the nearly 2:1 internal resonance between the 2nd S–I and 1st A–O modes is actually activable for involving a high-frequency symmetric in-plane mode [31] and, indeed, it plays an important role, as shown by the spatial shapes of the longitudinal and vertical responses of the excited 2nd S–I mode reported in Figs. 9(a) and (b), respectively ($T \approx 2.4-3.4$). The graphs in Figs. 8 and 9 confirm how the non-linear coupling is enhanced due to the internal resonance, which also entails a regularization of the in-plane response—towards which the energy is periodically transferred—with respect to cable B. In particular, the maximum amplitude of the out-of-plane response is reduced to about 0.79 times its initial value, whereas the maximum vertical amplitude rises from zero to about 33% of the maximum out-of-plane amplitude.

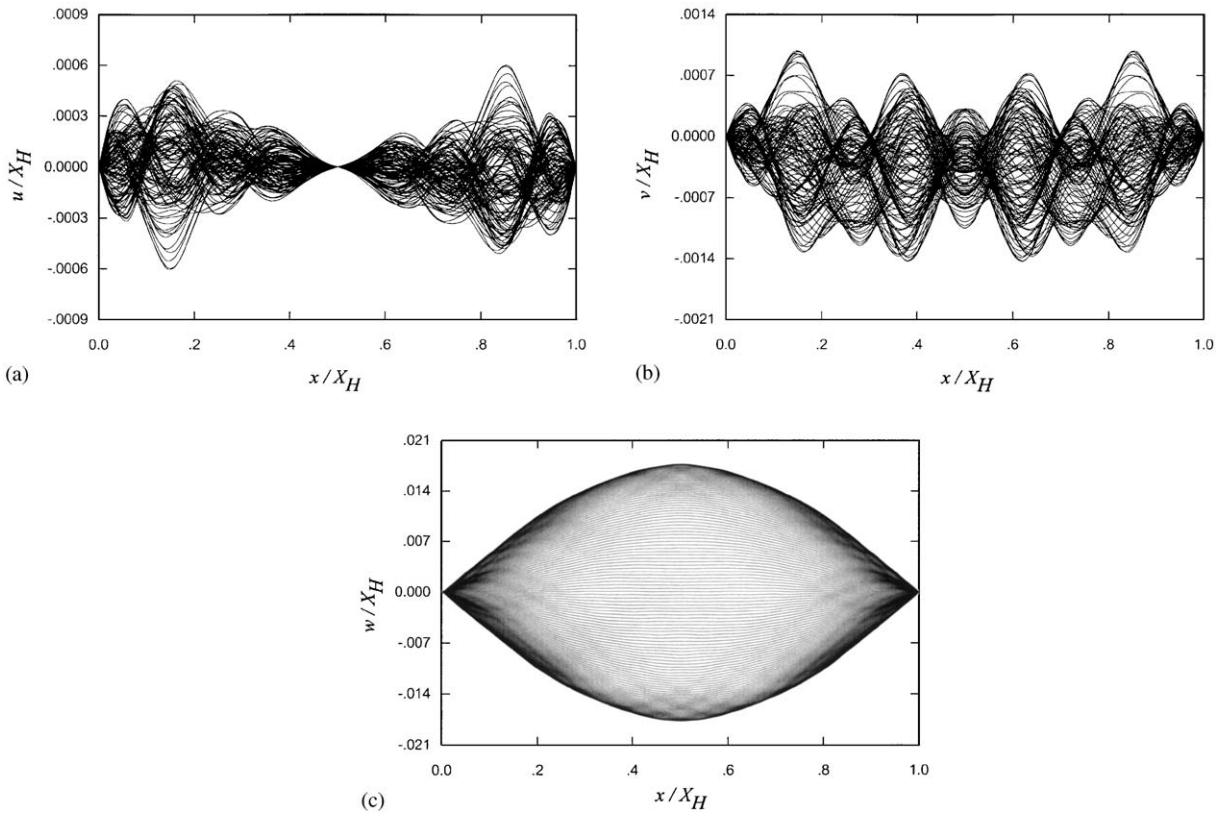

Fig. 7. Vibration profiles at different instants ($T \approx 6.0 - 6.5$) for cable D under initial condition of the 1st S–O mode: (a) longitudinal response; (b) vertical response; (c) out-of-plane response.

With the same initial amplitude, a combination of high-frequency components occurs again in the in-plane responses of cable D for which no internal resonance exists. The Fourier amplitude spectrum of the corresponding in-plane response is illustrated in Fig. 10 against those of cables B and C. The driven vertical responses of cables B and, mostly, D contain higher frequency components (Figs. 10(a) and (c)). Due to a 2:1 resonant condition, the vertical response of cable C has a single frequency (Fig. 10(b)), whose value (0.234 Hz) is approximately twice that of the out-of-plane one (0.117 Hz). These results highlight the fact that, apart from the regularizing effects entailed by the internal resonance condition, the in-plane response excited by the out-of-plane motion for a generic (non-resonant) cable is non-periodic, due to a combination of high-frequency components, irrespective of cable sag condition. The multi-harmonic longitudinal and vertical responses of cable D are displayed in Figs. 11(a) and (b) ($T \approx 4.0-4.5$) against the harmonic out-of-plane one (Fig. 11(c)), with the amplitude of the longitudinal response being now nearly comparable to that of the vertical one due to the large sag effect.

From the numerical results obtained in Section 4.1, non-zero values of vertical responses are obtained at cable mid-span. While highlighting that symmetric in-plane modes are excited by a prescribed out-of-plane mode, either symmetric or antisymmetric, this also confirms numerically

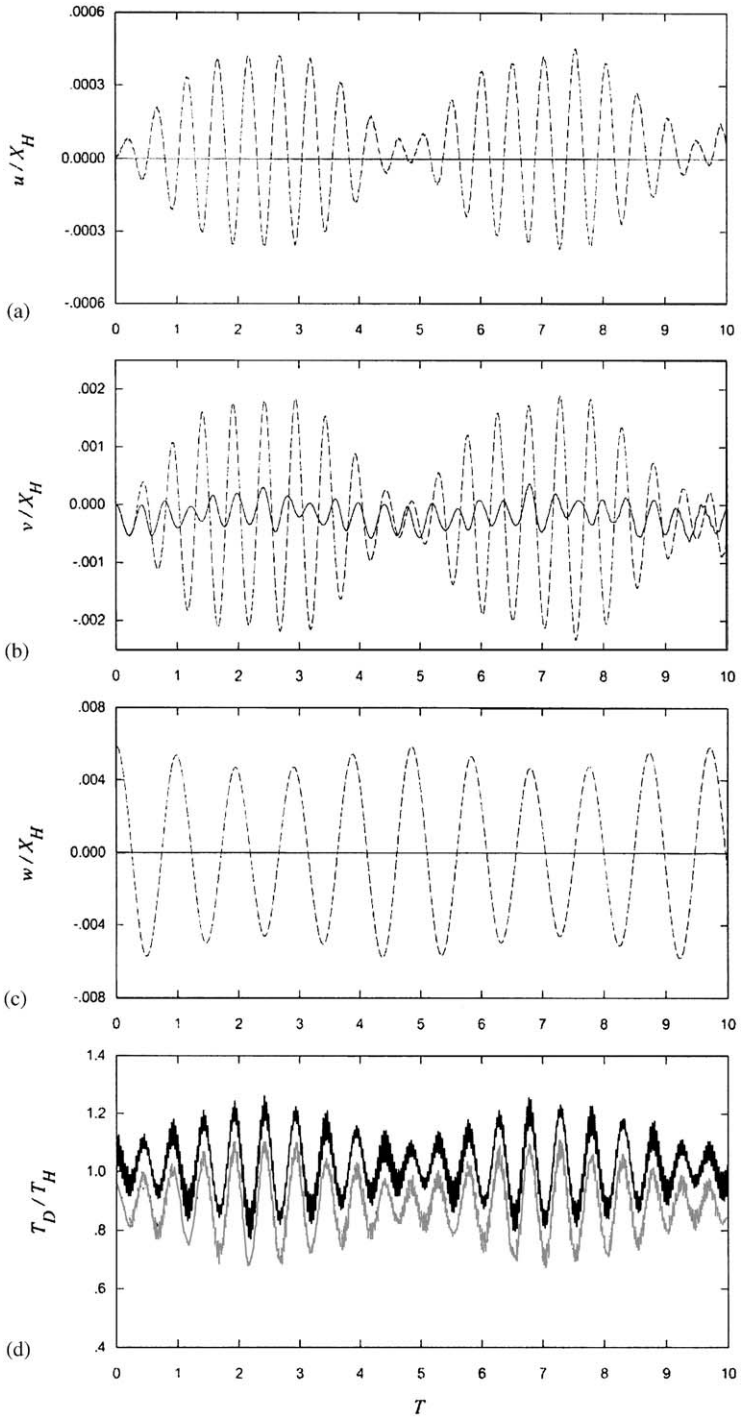

Fig. 8. Dynamic responses of cable C under initial condition of the 1st A–O mode: (a) longitudinal response; (b) vertical response; (c) out-of-plane response: —— mid-span, – – – quarter-span; (d) cable tension response: —— maximum, – – – minimum.

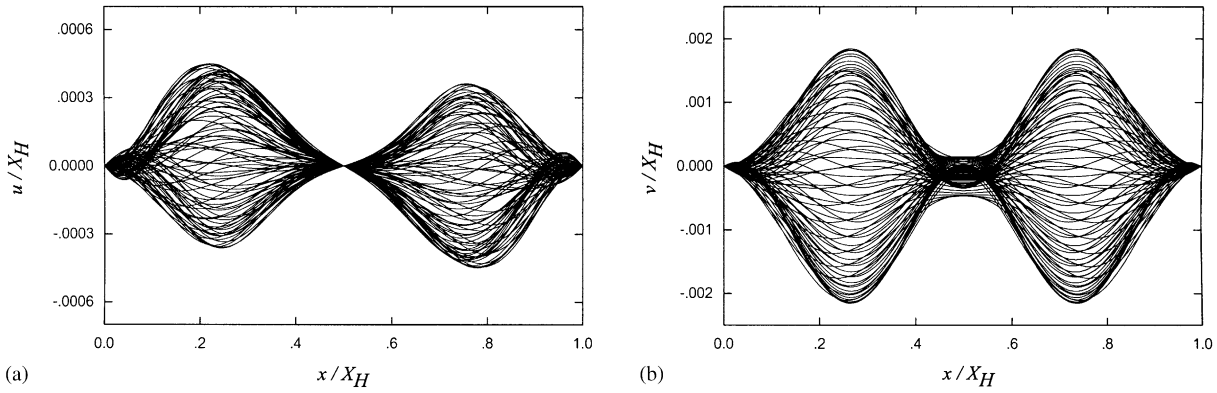

Fig. 9. Vibration profiles at different instants ($T \approx 2.4 - 3.4$) for cable C under initial condition of the 1st A–O mode: (a) longitudinal response; (b) vertical response.

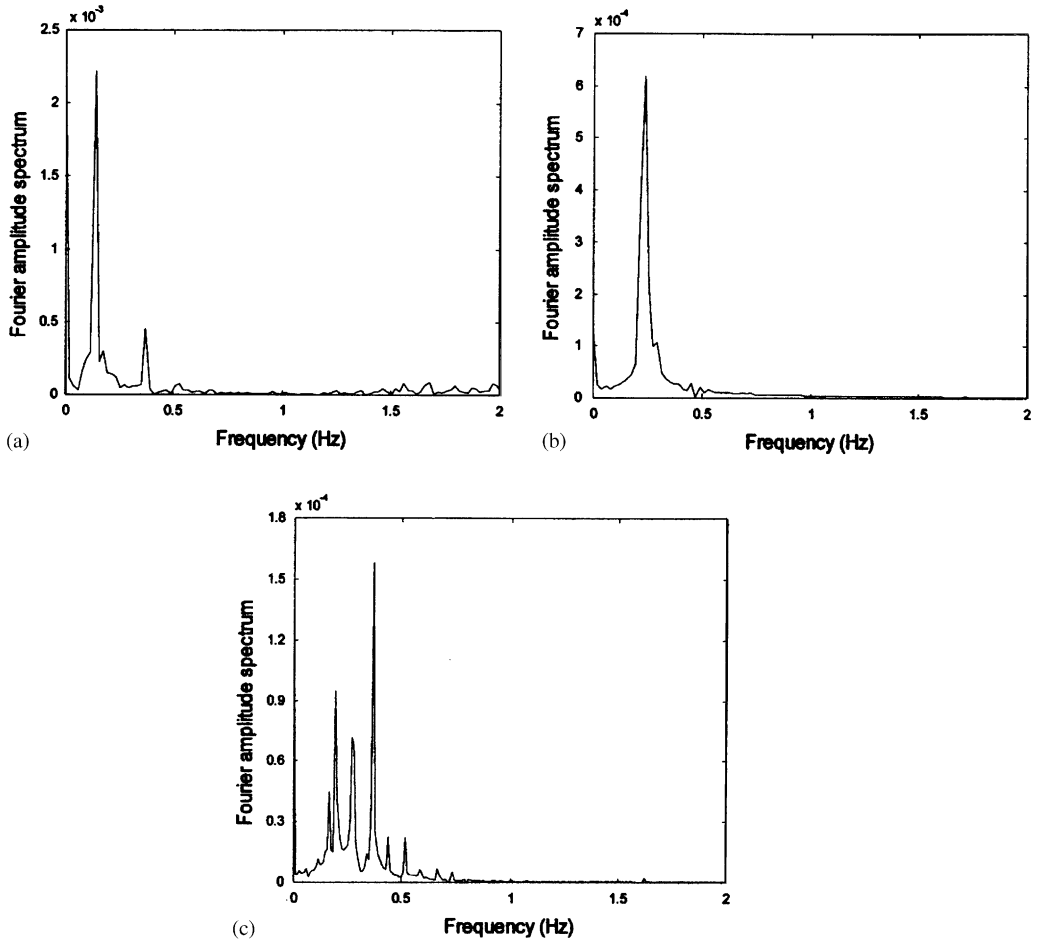

Fig. 10. Fourier amplitude spectra of cable vertical responses under initial condition of the 1st A–O mode: (a) cable B; (b) cable C; (c) cable D.

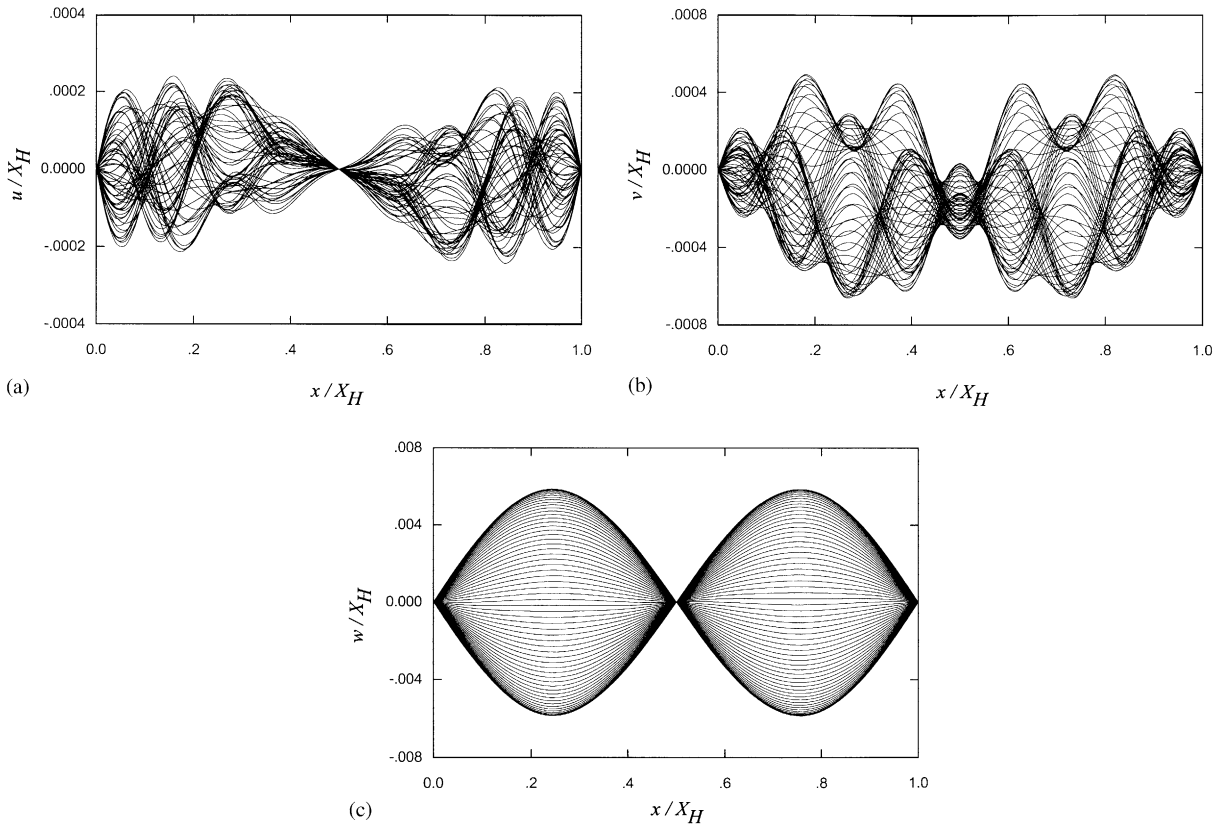

Fig. 11. Vibration profiles at different instants ($T \approx 4.0 - 4.5$) for cable D under initial condition of the 1st A–O mode: (a) longitudinal response; (b) vertical response; (c) out-of-plane response.

the theoretically predicted role [31] of symmetric in-plane modes in the actual activation of 2:1 internal resonances at crossover points. As regards cables with significant sag, it is worth noticing that the occurrence of a multi-harmonic response in the driven displacement components justifies the consideration of a m.d.o.f. cable model.

4.2. *Large-amplitude in-plane free vibrations*

Without any external excitation, no 3-D coupling occurs when only in-plane amplitude is initiated. This is because of the existence of monofrequent in-plane vibrations [2], consistent with the vanishing of all terms in the coupled equation of motion (Eq. (22)) when the variables corresponding to the out-of-plane displacement are set to zero. Nevertheless, there occur some interesting interaction behaviors, which are discussed below.

4.2.1. *First symmetric in-plane mode (1st S–I mode)*

When considering cable A with $\Delta = 15\,\text{m}$, the longitudinal responses are very low, the vertical responses are periodic, and the maximum tension has a steady maximum value greater than that

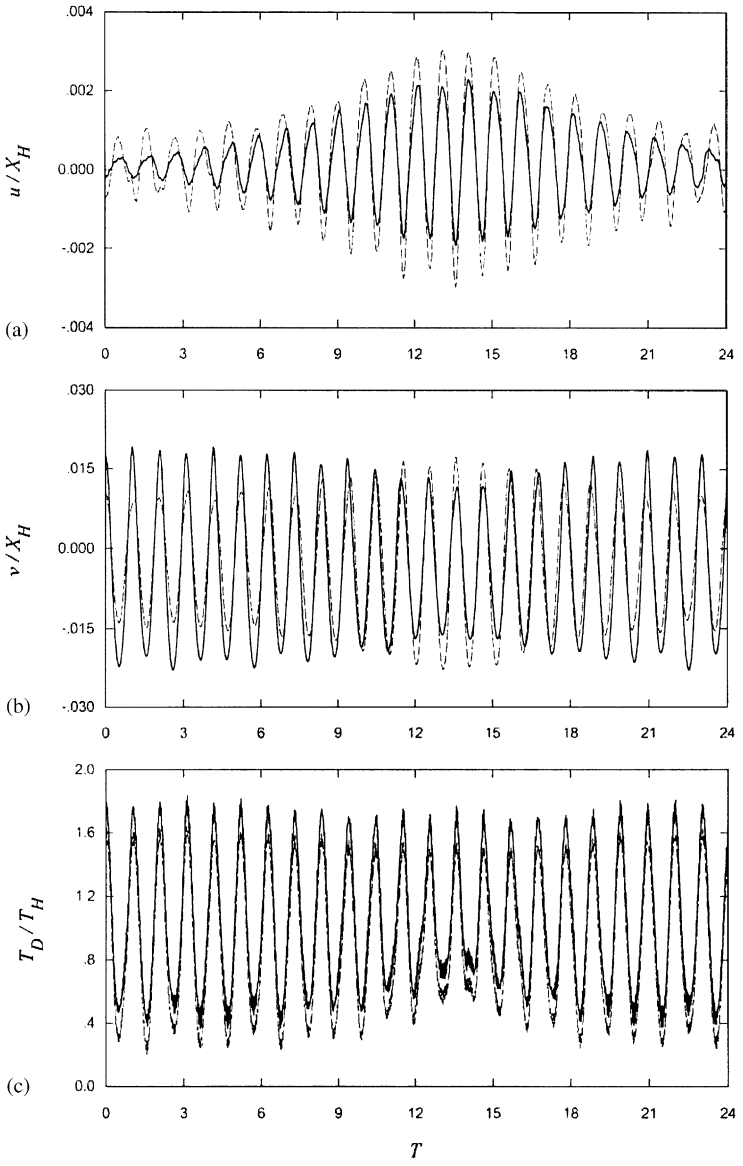

Fig. 12. Dynamic responses of cable B under initial condition of the 1st S–I mode: (a) longitudinal response; (b) vertical response: —— mid-span, – – – quarter span; (c) cable tension response: —— maximum, – – – minimum.

induced by the symmetric out-of-plane mode. In contrast, when considering cable B with the same initial amplitude, some outstanding characteristics are observed in the responses (Fig. 12). The vertical amplitude at mid-span, which is of course larger than the amplitude at quarter-span, is reduced evidently in some intervals ($T \approx 12 - 15$). Correspondingly, the longitudinal amplitude is increased due to a beating-like exchange. In contrast, both longitudinal and vertical amplitudes at quarter-span increase up to 4.74 and 2.00 times their initial values, respectively.

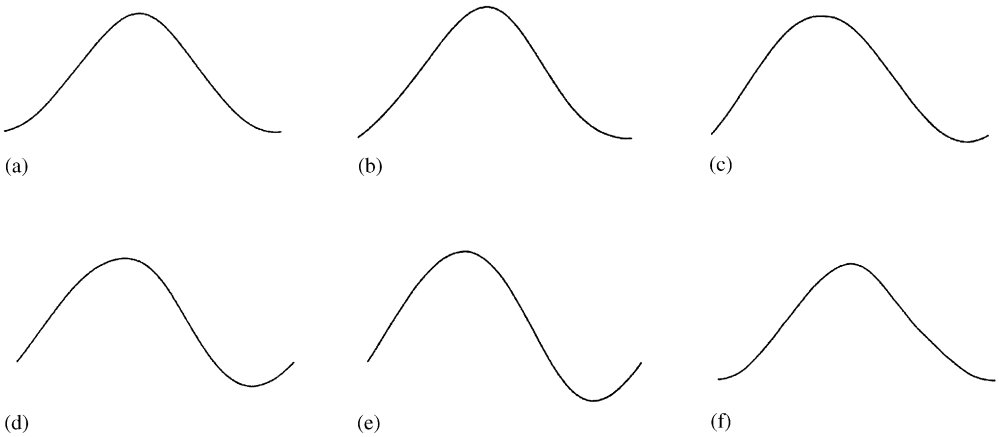

Fig. 13. Modal transition of cable B at different instants under initial condition of the 1st S–I mode: (a) $T \approx 2.1$; (b) $T \approx 5.2$; (c) $T \approx 8.4$; (d) $T \approx 10.5$; (e) $T \approx 12.6$; (f) $T \approx 23.0$.

For the sake of convenience, the transition of the vibration profile is shown to explain what occurs during this time duration. Only the dominant vertical displacements are displayed. As exemplified in Fig. 13, initially ($T \approx 2.1$) the vibration profile corresponds closely to the symmetric in-plane mode at the first crossover, namely it is tangential to the equilibrium cable profile at each support (Fig. 13(a)). The associated antisymmetric longitudinal displacement is nearly zero at mid-span. Then, the vibration profile evolves smoothly towards a hybrid asymmetric shape (Figs. 13(d) and (e)) which accounts for a superimposition of the first symmetric and antisymmetric modes. Accommodation of the latter into the response ensues from cable B corresponding to a perfectly tuned 1:1 internal resonance between the two in-plane modes and from 1:1 internal resonances being always activable at crossover points [31]. Due to the antisymmetric vertical displacement accompanied by a symmetric longitudinal one with maximum value at quarter-span [30], the simultaneous increase of both corresponding amplitudes in Figs. 12(a) and (b) is explained. Afterwards, the vibration profile returns back to the symmetric mode ($T \approx 23.0$, Fig. 13(f)). In turn, the tension responses—which attain rather large values, on average—change slightly when the hybrid mode phenomenon takes place (Fig. 12(c)). The previous results further confirm some points made in the literature (see, e.g., Refs. [11,14]) about the antisymmetric mode being driven in the response by an existing symmetric one due to non-linear modal coupling and a mechanism of induced dynamic tension. The difference here is that the in-plane coupled dynamics are non-stationary.

Exciting the large-sagged cable D with a reduced initial amplitude ($\Delta = 5\,\text{m}$), the longitudinal and vertical responses are slightly disturbed by high-frequency components. This implies that the cable sag has an influence also on the in-plane response besides the out-of-plane one. Moreover, the difference in magnitude occurring between maximum and minimum tensions (Fig. 14) justifies the need to take into account strain variations in the non-linear cable model.

4.2.2. First antisymmetric in-plane mode (1st A–I mode)

No special features are observed in the dynamic response of the 1:1 resonant cable B with $\Delta = 15\,\text{m}$, different from the previous case of excitation with symmetric mode, in particular no

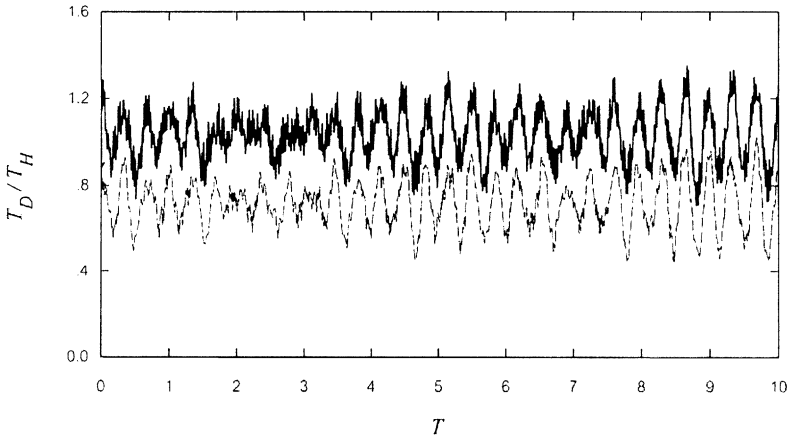

Fig. 14. Cable tension responses of cable D under initial condition of the 1st S–I mode: —— maximum, – – – minimum.

other modes enter the response. Considering cable C with $\Delta = 5$ m, the beating phenomenon is clearly observed in the force responses (Fig. 15(c)), while some noteworthy characteristics occur in the displacement time histories, too (Figs. 15(a) and (b)). The observed behavior is governed by a kind of internal resonance existing at the second crossover. The vibration profiles at different times are displayed comparatively in Fig. 16. Evidently, the shape of vertical response evolves from the initial antisymmetric mode, occurring when $T \approx 1.0$ (Fig. 16(a)), to the second symmetric mode (Fig. 16(b)), up to a hybrid profile accounting for the two modes when $T \approx 4.7$ (Fig. 16(d)). Then, the shape returns to the second symmetric mode (Fig. 16(e)), and eventually develops to become again the original antisymmetric mode when $T \approx 6.7$ (Fig. 16(f)). Thus, Fig. 16 reveals how the 2nd S–I mode is excited and accommodated into the response initiated by the 1st A–I mode due to their involvement in a 1:2 internal resonance, which is again activated because of the higher-frequency mode being symmetric [31]. This higher mode is seen to substantially dominate the cable vibration profile in some intervals of the considered time stepping, and to cause meaningful increases in the magnitude of cable tension responses (Fig. 15(c)). The non-linear frequencies dominating the longitudinal and vertical responses are evaluated using the Fourier amplitude spectral densities, as shown in Figs. 17(a) and (b). They are approximately equal to 0.115 and 0.225 Hz, thus being both greater than the corresponding linear frequencies of first antisymmetric and second symmetric modes (Table 1), respectively: the system is thus seen to exhibit a weakly hardening non-linear behavior.

Two points are worth noticing for the present cable C at the second crossover, where various internal resonances occur. (i) The (coexisting) 2:1 resonance between the 2nd A–I mode and the initiated 1st A–I mode does not play any role, which ensues from the activation of 2:1 in-plane resonances requiring contribution from at least one (higher-frequency) symmetric mode [31]. (ii) The activable 1:1 internal resonance involving the 2nd S–I and 2nd A–I modes—and characterizing the second crossover—also occurs, but it does not play any role, too, since the 1st A–I mode is initiated. Consequently, it seems worth analyzing how the motion behaves when applying the 2nd S–I mode as the initial condition, instead. Fig. 18 shows the overall responses

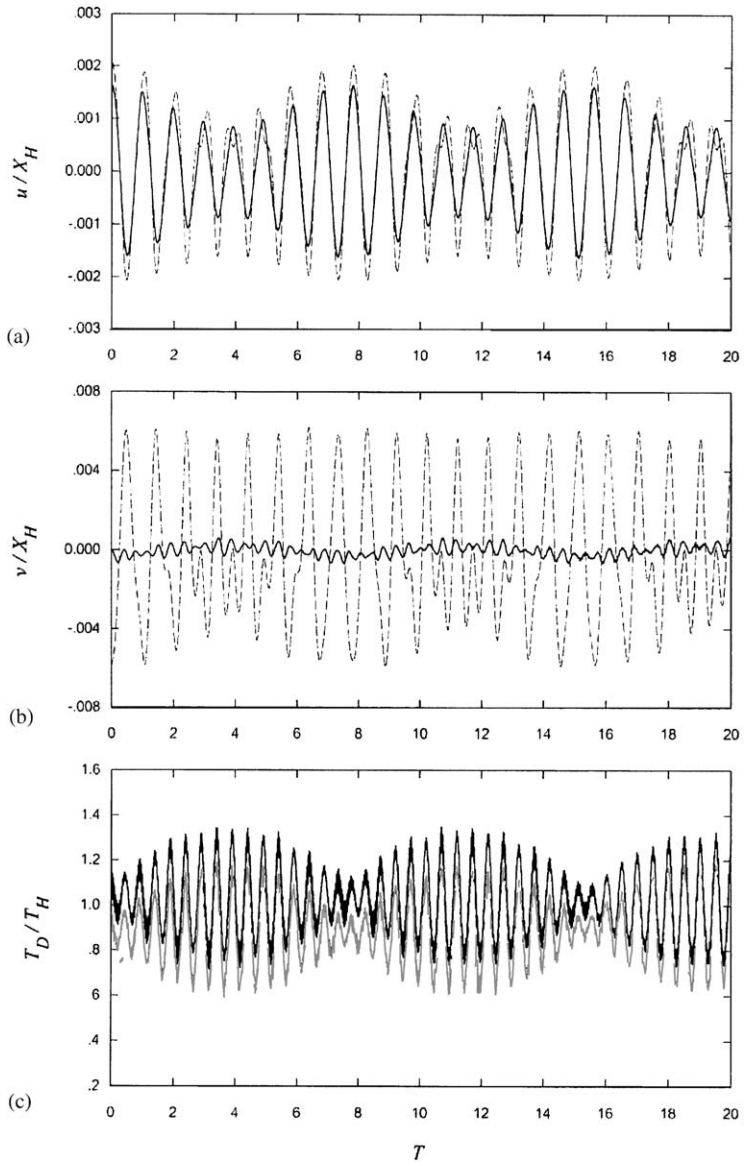

Fig. 15. Dynamic responses of cable C under initial condition of the 1st A–I mode: (a) longitudinal response; (b) vertical response: —— mid-span, – – – quarter span; (c) cable tension response: —— maximum, – – – minimum.

under this initiation with the same assigned amplitude ($\Delta = 5\,\mathrm{m}$) as before. Two interesting features are observed. (i) The longitudinal and vertical amplitudes at quarter-span are both increased to about 3.23 and 1.54 times their initial value, respectively; (ii) correspondingly, the relevant non-linear frequencies both decrease.

To explain the first point, the transition of the vibration profiles associated with the vertical amplitudes is displayed in Fig. 19 for those particular time intervals. Starting from $T \approx 11.4$, the

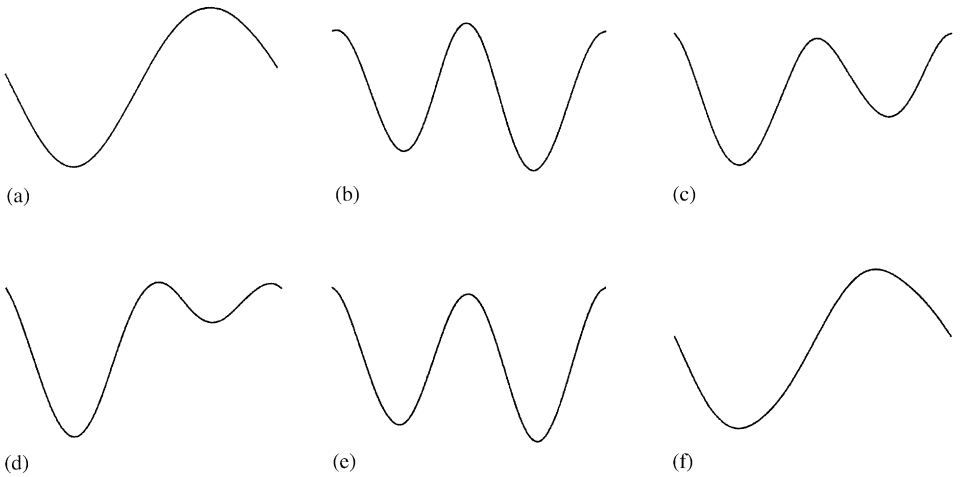

Fig. 16. Modal transition of cable C at different instants under initial condition of the 1st A–I mode: (a) $T \approx 1.0$; (b) $T \approx 2.7$; (c) $T \approx 3.7$; (d) $T \approx 4.7$; (e) $T \approx 5.1$; (f) $T \approx 6.7$.

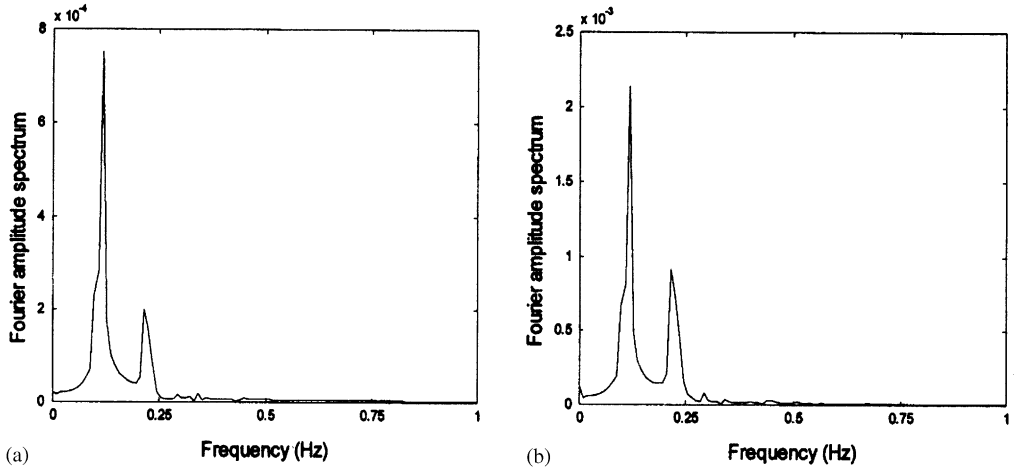

Fig. 17. Fourier amplitude spectra of cable C under initial condition of the 1st A–I mode: (a) longitudinal response at quarter span; (b) vertical response at quarter span.

profile corresponds to the 2nd S–I mode (Fig. 19(a)), then it evolves to a hybrid profile when $T \approx 20.7$ (Fig. 19(b)), up to changing completely into the 1st A–I mode when $T \approx 22.6$ and 24.3 (Figs. 19(c) and (d)). After attaining a further hybrid shape (Fig. 19(e)), the 2nd S–I mode resettles again at $T \approx 30.4$ (Fig. 19(f)). This phenomenon of modal transition repeats itself as long as no external disturbance is imposed on the cable. Thus, Fig. 19 reveals how the lower order antisymmetric mode is excited and accommodated into the cable response due to the 2:1 internal resonance condition. During the time interval where the vertical profile coincides approximately with the antisymmetric mode, the cable tension in Fig. 18(c) diminishes by about 40% with respect to its maximum value, as expected from the linear theory since antisymmetric modes entail

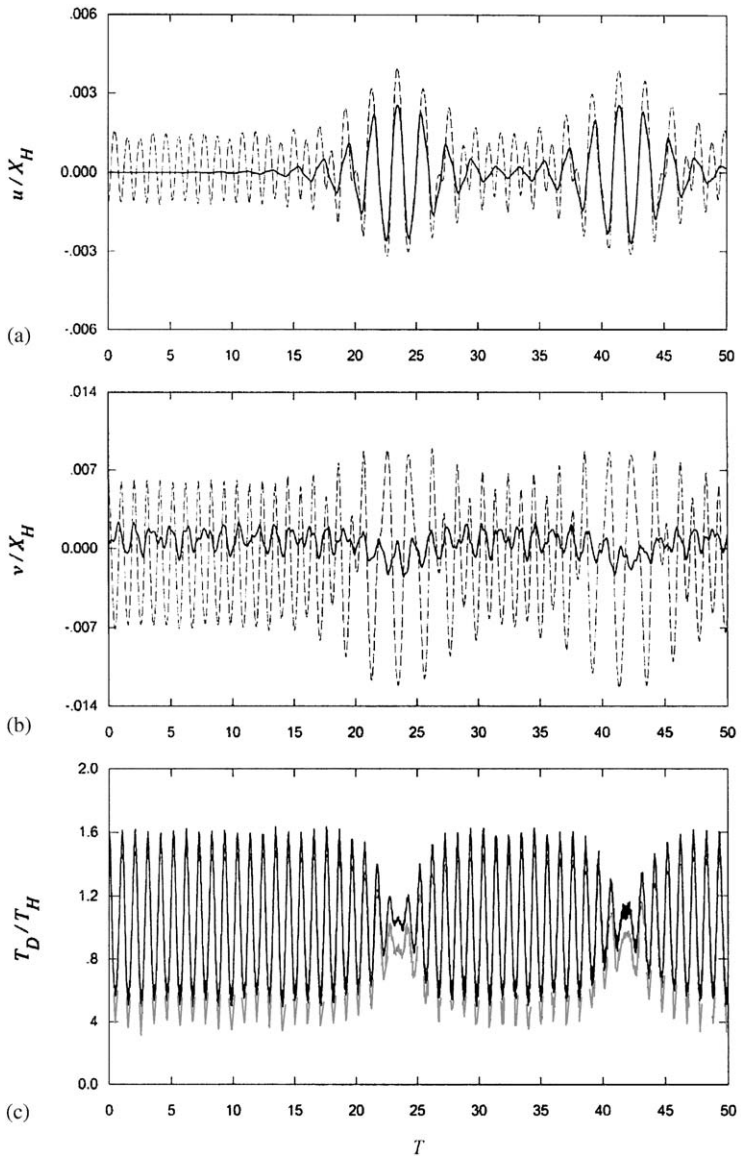

Fig. 18. Dynamic responses of cable C under initial condition of the 2nd S–I mode: (a) longitudinal response; (b) vertical response: —— mid-span, – – – quarter span; (c) cable tension response: —— maximum, – – – minimum.

no first order axial stretching. The obtained results (Figs. 18 and 19) are substantially the reverse of those in Figs. 15 and 16, with the role of the two involved modes being exchanged with each other during the transition interval. A difference is represented by the amplitude decrease (increase) of both the longitudinal and vertical responses occurring in the transition interval when the first antisymmetric (second symmetric) mode is initiated. Besides ensuing from the specific profile changes, it also expresses the circumstance of the 2nd S–I mode being more constrained

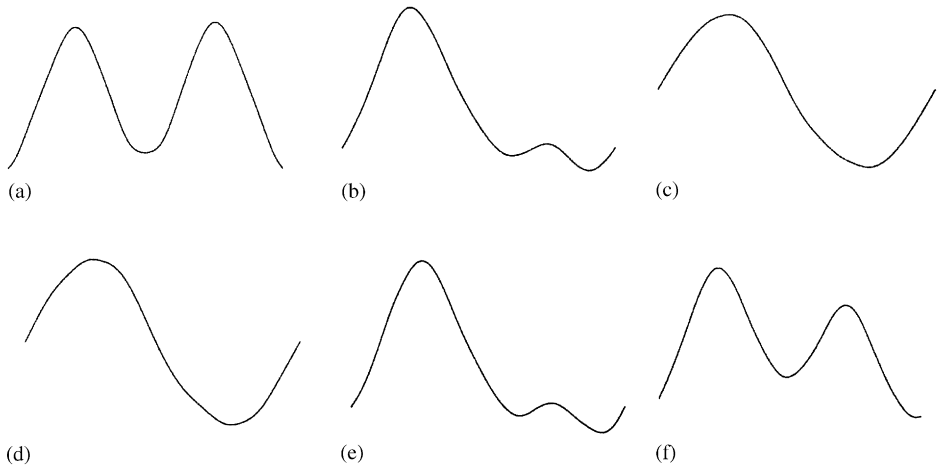

Fig. 19. Modal transition of cable C at different instants under initial condition of the 2nd S–I mode: (a) $T \approx 11.4$; (b) $T \approx 20.7$; (c) $T \approx 22.6$; (d) $T \approx 24.3$; (e) $T \approx 26.3$; (f) $T \approx 30.4$.

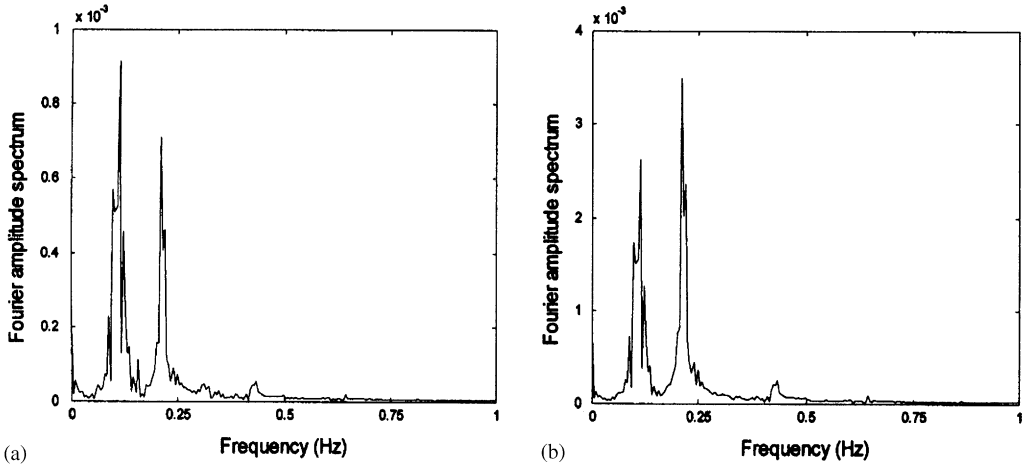

Fig. 20. Fourier amplitude spectra of cable C under initial condition of the 2nd S–I mode: (a) longitudinal response at quarter span; (b) vertical response at quarter span.

than the 1st A–I one, which entails a lower amplitude of the former with respect to the latter at a given energy level. Thus, one can conclude that the dominant internal resonance is the 2:1 one even when initiating the 2nd S–I mode. The possible activation of the 2nd A–I mode involved in the 1:1 resonance with the excited symmetric one does not actually occur, since the 2:1 resonance usually dominates instead of the coexisting 1:1 [14].

To check the frequency of longitudinal and vertical responses in the transition interval, the Fourier amplitude spectra are illustrated (Figs. 20(a) and (b)). The non-linear frequencies are equal to 0.107 and 0.210 Hz, approximately, and denote a weakly softening non-linear behavior, contrary to the first antisymmetric initiation. Phase-plane portraits are also reported in Fig. 21,

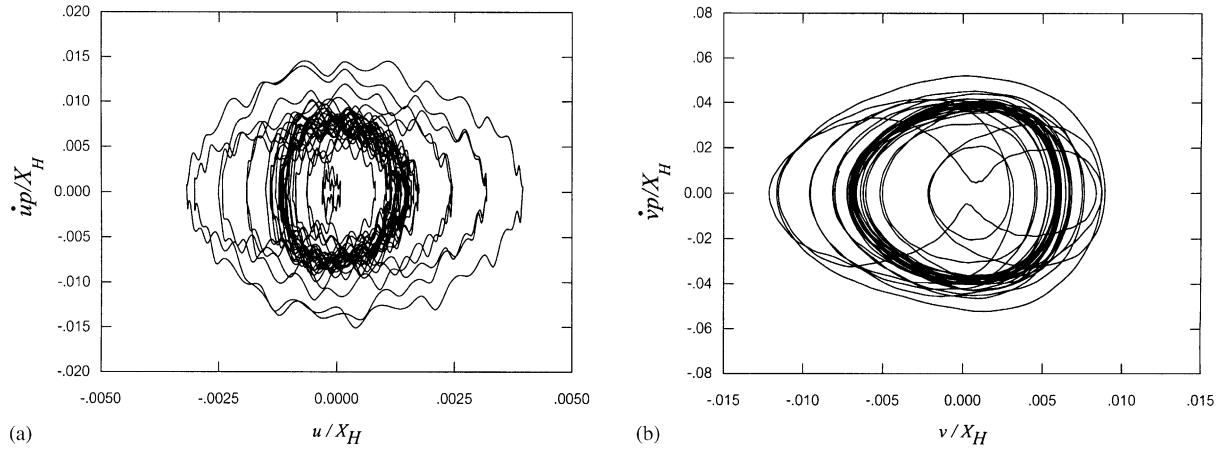

Fig. 21. Phase-plane portraits of cable C under initial condition of the 2nd S–I mode: (a) longitudinal response at quarter span; (b) vertical response at quarter span.

whose variable p in the vertical axis is the linear period of the initiated mode. They exhibit elliptical trajectories of maximum displacements with features of amplitude modulation of both longitudinal and vertical responses, as well as of small perturbations of the former. Fig. 21 shows how the energy of the motion changes through the dominant resonant condition, namely the inner repeated ellipses indicate the motion on the second symmetric mode, whereas the outer ellipses correspond to the first antisymmetric mode.

This section is concluded with a further short comment about numerical checks on possible activation/non-activation of coexisting internal resonances. Another cable yet to be referred (not reported in Table 1) corresponds to the 3rd crossover point (namely, $\lambda/\pi = 6$) of in-plane frequencies. In such a case, theoretical predictions [31] suggest that the 3:1 resonance occurring between 3rd S–I mode ($\omega \approx 0.281$ Hz) and 1st A–I mode ($\omega \approx 0.094$ Hz) is not activable because the involved modes are of a different type (symmetric–antisymmetric), whereas the 2:1 resonance between 3rd S–I and 1st S–I ($\omega \approx 0.141$ Hz) could be activated since it involves two symmetric modes. Numerical results confirm these predictions, as highlighted in Figs. 22 and 23. The former shows the overall responses of this new cable due to 3rd S–I initiation; the vibration profiles in the latter show the accommodation of the 1st S–I mode (Fig. 23(d)) in the response dominated by the 3rd S–I mode (Figs. 23(a) and (f)), within the transition interval of Figs. 22(b) and (c) where the vertical amplitude at mid-span increases and the dynamic tension decreases.

5. Conclusions

A 3-D model formulation capable of analyzing the large-amplitude free vibrations of a suspended cable has been developed. According to a m.d.o.f. model of cable, which accounts for the axial deformation effect, the formulation is not restricted to cables having small sag-to-span ratios. A finite difference discretization of the equations of motion in both space and time has

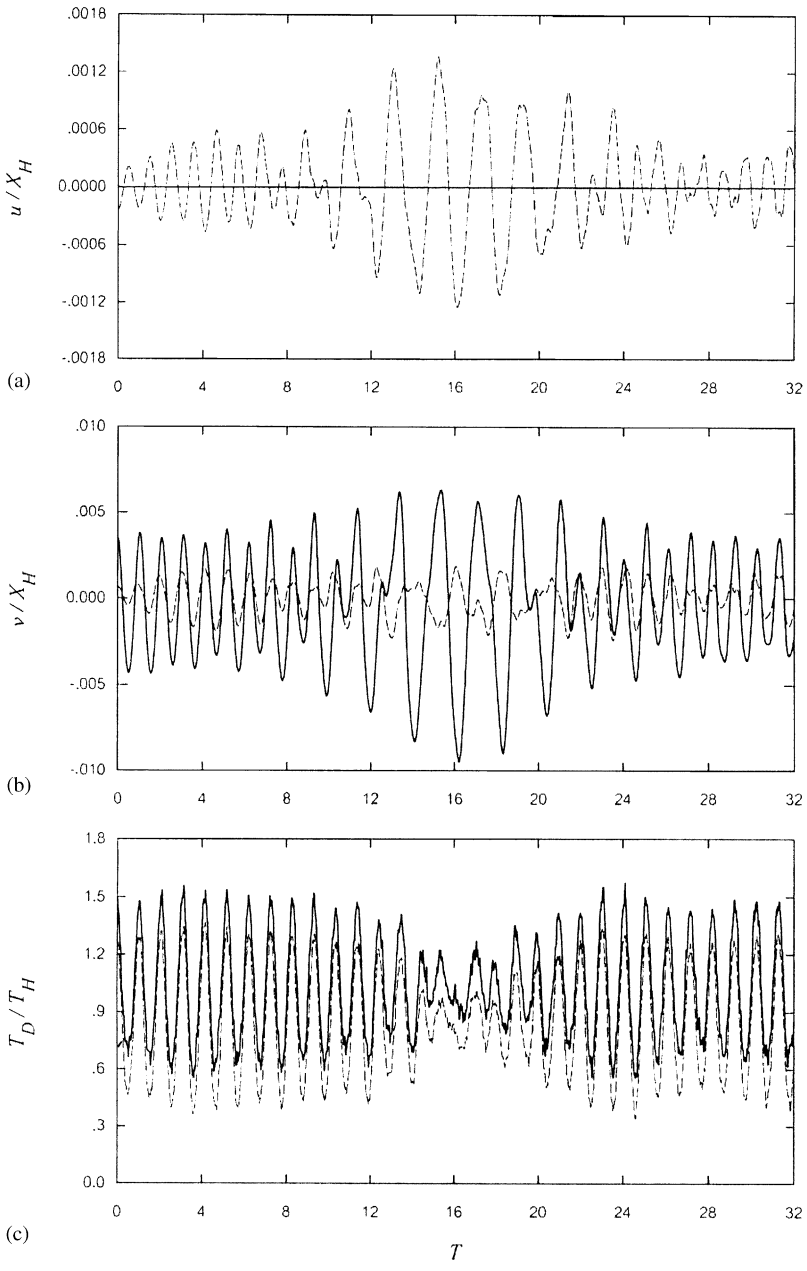

Fig. 22. Dynamic responses of cable corresponding to the 3rd crossover point ($\lambda/\pi \approx 6$) under initial condition of the 3rd S–I mode: (a) longitudinal response; (b) vertical response: —— mid-span, – – – quarter span; (c) cable tension response: —— maximum, – – – minimum.

been performed and numerically implemented to obtain time histories of non-linear dynamic response. Numerous examples of cables subjected to initial large-amplitude out-of-plane or in-plane vibrations have been discussed in the case of a specified end tension.

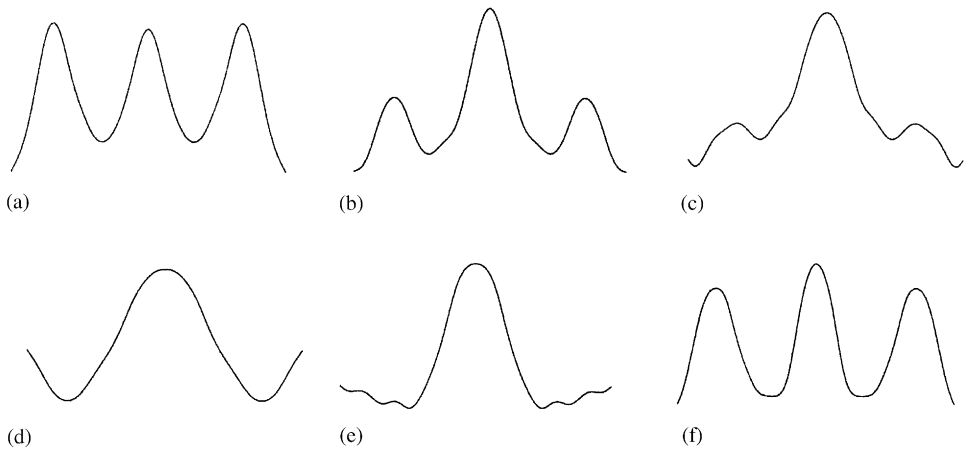

Fig. 23. Modal transition of cable corresponding to the 3rd crossover point ($\lambda/\pi \approx 6$) at different instants under initial condition of the 3rd S–I mode: (a) $T \approx 6.2$; (b) $T \approx 9.3$; (c) $T \approx 11.3$; (d) $T \approx 15.3$; (e) $T \approx 19.0$; (f) $T \approx 28.2$.

Based on the analysis results, the following points on cable non-linear behaviors are drawn, in the case of out-of-plane initial displacement conditions.

- Symmetric in-plane modes are excited irrespective of the initiating out-of-plane motion being symmetric or antisymmetric, with the latter case involving higher symmetric modes.
- Regardless of cable sag condition, the driven in-plane response of a non-resonant cable is non-periodic, unlike the periodically driven response of an internally resonant cable. In turn, non-linear 3-D coupling is enhanced by the occurrence of an internal resonance condition.
- The cable tension is augmented mostly due to the occurrence of increased in-plane vibration amplitudes, and is further enhanced when the cable exhibits internally resonant frequencies.
- For a cable sagging significantly, the cable vibration profiles exhibit qualitatively multi-harmonic responses due to geometric non-linearities: this accounts for the need to consider m.d.o.f. cable models. In addition, the longitudinal response tends to become nearly comparable to the vertical one, though being an order of magnitude lower than that for low-sagged cables.

In the case of in-plane initial displacement conditions, depending on driving mode and on magnitude of specified initial amplitude, worthwhile phenomena of modal transition may take place for crossover cables during the ensuing in-plane vibrations. Indeed, due to the occurrence of a dominant internal resonance, a higher or lower mode can be accommodated into the response initiated by a single mode, making the cable vibration profile hybrid in some intervals of the considered time marching. Besides the well-known 1:1 internally resonant cable at the first crossover, whose first antisymmetric mode is excited when the first symmetric mode is initiated, various modal transition phenomena occur for 2:1 resonant cables. E.g., at the second crossover, the second symmetric (first antisymmetric) mode is excited when the first antisymmetric (second symmetric) mode is initiated: the excited symmetric (antisymmetric) mode may dominate substantially the cable vibration profile, as well as induce meaningful increase (decrease) in the

magnitude of cable tension responses. Moreover, the difference in magnitude between maximum and minimum tensions increases for a cable with significant sag, which highlights the need to account for strain variation in the cable model.

All of the numerical results obtained for cables at crossovers have been discussed against the background of the theoretical predictions about activation of 1:1 or 2:1 internal resonances made within an infinite dimensional analytical framework [31]. Besides highlighting the dynamic effects entailed by their actual activation, numerical results provide worthwhile information about which one of the coexisting internal resonances actually governs the system dynamics.

Acknowledgements

The authors gratefully acknowledge the financial support of the Thailand Research Fund (TRF) under Grants PHD/0167/2543 and RTA/03/2543.

References

[1] P. Hagedorn, B. Schafer, On non-linear free vibrations of an elastic cables, International Journal of Non-linear Mechanics 15 (1980) 333–340.
[2] A. Luongo, G. Rega, F. Vestroni, Monofrequent oscillations of a non-linear model of a suspended cable, Journal of Sound and Vibration 82 (1982) 247–259.
[3] A. Luongo, G. Rega, F. Vestroni, Planar non-linear free vibrations of an elastic cable, International Journal of Non-linear Mechanics 19 (1984) 39–52.
[4] G. Rega, F. Vestroni, F. Benedettini, Parametric analysis of large amplitude free vibrations of a suspended cable, International Journal of Solids and Structures 20 (1984) 95–105.
[5] F. Benedettini, G. Rega, F. Vestroni, Modal coupling in the free nonplanar finite motion of an elastic cable, Meccanica 21 (1986) 38–46.
[6] F. Benedettini, G. Rega, Non-linear dynamics of an elastic cable under planar excitation, International Journal of Non-linear Mechanics 22 (1987) 497–509.
[7] G. Rega, F. Benedettini, Planar non-linear oscillations of elastic cables under subharmonic resonance conditions, Journal of Sound and Vibration 132 (1989) 367–381.
[8] G.V. Rao, R.N. Iyengar, Internal resonance and non-linear response of a cable under periodic excitation, Journal of Sound and Vibration 149 (1991) 25–41.
[9] N.C. Perkins, Modal interactions in the non-linear response of elastic cables under parametric/external excitation, International Journal of Non-linear Mechanics 27 (1992) 233–250.
[10] C.L. Lee, N.C. Perkins, Nonlinear oscillations of suspended cables containing a two-to-one internal resonance, Nonlinear Dynamics 3 (1992) 465–490.
[11] C.L. Lee, N.C. Perkins, Three-dimensional oscillations of suspended cables involving simultaneous internal resonances, Nonlinear Dynamics 8 (1995) 45–63.
[12] F. Benedettini, G. Rega, R. Alaggio, Nonlinear oscillations of a four-degree-of freedom model of a suspended cable under multiple internal resonance conditions, Journal of Sound and Vibration 182 (1995) 775–798.
[13] G. Rega, R. Alaggio, F. Benedettini, Experimental investigation of the nonlinear response of a hanging cable Part I: Local analysis, Nonlinear Dynamics 14 (1997) 89–117.
[14] F. Benedettini, G. Rega, Experimental investigation of the nonlinear response of a hanging cable. Part II: Global analysis, Nonlinear Dynamics 14 (1997) 119–138.
[15] M. Behbahani-Nejad, N.C. Perkins, Freely propagating waves in elastic cables, Journal of Sound and Vibration 196 (1996) 189–202.

[16] M. Pakdemirli, S.A. Nayfeh, H.A.H. Nayfeh, Analysis of one-to-one autoparametric resonance in cables-discretization vs. direct treatment, Nonlinear Dynamics 8 (1995) 65–83.
[17] G. Rega, W. Lacarbonara, A.H. Nayfeh, C.M. Chin, Multiple resonances in suspended cables: direct versus reduced-order models, International Journal of Non-linear Mechanics 34 (1999) 901–924.
[18] J.V. Huddleston, Computer analysis of extensible cables, Journal of Engineering Mechanics, American Society of Civil Engineers 107 (1981) 27–37.
[19] B. Shih, I.G. Tadjbakhsh, Small-amplitude vibrations of extensible cables, Journal of Engineering Mechanics, American Society of Civil Engineers 110 (1984) 569–576.
[20] J.J. Burgess, M.S. Triantafyllou, The elastic frequencies of cables, Journal of Sound and Vibration 120 (1988) 153–165.
[21] M.S. Triantafyllou, D.K.P. Yue, Damping amplification in highly extensible hysteretic cables, Journal of Sound and Vibration 186 (1995) 355–368.
[22] A.A. Tjavaras, Q. Zhu, Y. Liu, M.S. Triantafyllou, D.K.P. Yue, The mechanics of highly extensible cables, Journal of Sound and Vibration 213 (1998) 709–737.
[23] S. Chucheepsakul, S. Wongsa, Effect of axial stretching on large amplitude free vibration of a suspended cable, Structural Engineering and Mechanics 11 (2001) 185–197.
[24] S. Chucheepsakul, N. Srinil, Free vibrations of three-dimensional extensible marine cables with specified top tension via a variational method, Ocean Engineering 29 (2002) 1067–1097.
[25] W.M. Henghold, J.J. Russell, Equilibrium and natural frequencies of cable structures (a nonlinear finite element approach), Computers and Structures 6 (1976) 271–276.
[26] F. Rosenthal, Vibrations of slack cables with discrete masses, Journal of Sound and Vibration 78 (1981) 573–583.
[27] K. Takahashi, Y. Konishi, Non-linear vibrations of cables in three dimensions. Part 1: Non-linear free vibrations, Journal of Sound and Vibration 118 (1987) 69–84.
[28] A.C.J. Luo, C.D. Mote Jr., Equilibrium solutions and existence for traveling, arbitrarily sagged elastic cables, American Society of Mechanical Engineers, Journal of Applied Mechanics 67 (2000) 148–154.
[29] S. Chucheepsakul, N. Srinil, P. Petchpeart, A variational approach for three-dimensional model of extensible marine cables with specified top tension, Applied Mathematical Modelling 27 (2003) 781–803.
[30] H.M. Irvine, T.K. Caughey, The linear theory of free vibrations of a suspended cable, Proceedings of the Royal Society of London Series A 341 (1974) 229–315.
[31] W. Lacarbonara, G. Rega, Resonant nonlinear normal modes. Part II: Activation/orthogonality conditions for shallow structural systems, International Journal of Non-linear Mechanics 38 (2003) 873–887.